ARTICLE

Journal of Materials Chemistry
www.rsc.org/materials

Spirobifluorene-based pyrazoloquinolines: efficient blue electroluminescent materials†

Ching-Hsin Chen,[a] Fang-Iy Wu,[a] Ching-Fong Shu,*[a] Chin-Hsiung Chien[b] and Yu-Tai Tao*[b]

[a]*Department of Applied Chemistry, National Chiao Tung University, Hsin-Chu, Taiwan 30035*
[b]*Institute of Chemistry, Academia Sinica, Taipei, Taiwan 11529*

Received 19th February 2004, Accepted 22nd March 2004
First published as an Advance Article on the web 22nd April 2004

We report the synthesis of spirobifluorene-based pyrazoloquinolines, spiro-**PAQ-Me** and spiro-**PAQ-Ph**, in which two identical luminophores are connected through an sp^3-hybridized carbon atom (a spiro center) and are orthogonally arranged. The incorporation of the rigid spirobifluorene linkage results in significant increases in the glass transition temperatures, which are in the range 246–280 °C. These new materials display the characteristic absorptions of the mono-pyrazoloquinoline (*i.e.* non-spiro) derivatives, each with a broad, low-energy absorption at *ca.* 420 nm, and emit photoluminescence efficiently in the blue region. Electrochemical studies reveal that these compounds exhibit reversible reductions and low-lying LUMO energy levels that originate from the electron-deficient nature of the pyrazoloquinoline ring. Multilayer organic electroluminescent devices constructed using spiro-**PAQ-Ph** as a dopant in the emitting layer produced bright blue emissions with maximum luminescence exceeding 20 000 cd m^{-2}. For the 2.0%-doped device, a high external quantum efficiency of 3.6% (4.5 cd A^{-1}, 2.02 lm W^{-1}) was achieved at 20 mA cm^{-2} and 7.0 V with color coordinates of (0.14, 0.17).

Introduction

Since the discovery of multi-layered organic light-emitting diodes (OLEDs) by Tang and Van Slyke,[1] research into OLEDs has been pursued intensively because of their potential for applications in, among other things, flat-panel displays.[2–6] With such an application in mind, full-color displays would require three primary-color emissions, *i.e.* red, green, and blue. Organic light-emitting materials having large band-gap energies that emit blue light efficiently are of particular interest, because they are desired for use as blue light sources in full-color display applications and also because they can be used to achieve green and red color emission by several pathways, such as dopant emission or fluorescent down-conversion.[7–10] A range of pyrazole-containing derivatives have been demonstrated to exhibit efficient blue photoluminescence,[11–13] and some of them have been utilized as emitting materials in the fabrication of electroluminescent (EL) devices, in which they provide bright blue EL emission.[14–21]

Herein, we report the synthesis and characterization of spirobifluorene-based pyrazoloquinolines, in which the two identical luminophores are aligned orthogonally through bonding to an sp^3-hybridized carbon atom: a spiro center.[22,23] The introduction of a spirobifluorene linkage not only increases molecular rigidity but also hinders close packing and intermolecular interactions, so that the tendency for molecules to crystallize may be reduced and the glass transition temperature may be increased.[24–29] Amorphous materials possessing a high value of T_g, which are less vulnerable to heat-induced morphological changes, are highly desirable for fabricating molecular LEDs, since the tendency for small molecules to crystallize spontaneously during operation has been identified as one reason for LED device failure.[30–35] Moreover, the tetrahedral nature of the carbon atom at the spiro center connects the conjugated moieties through a σ-bonded network, which in turn serves as a conjugation interrupt, and, thus, most of the desired electronic and optical properties of the corresponding non-spiro molecules are preserved.[29,36,37] The spirobifluorene-based pyrazoloquinoline was used as a dopant in EL devices, which gave bright blue emission from the dopant. The performance of these devices is discussed.

Experimental

General

2,2′-Dinitro-9,9′-spirobifluorene (**1**),[38] 9,9-spirobifluorene-bis-3-phenyl[2,3-*c*]isoxazole (**2**),[36] and 2,2′-diamino-3,3′-dibenzoyl-9,9′-spirobifluorene (**3**)[36] were synthesized according to literature procedures. Tetrabutylammonium hexafluorophosphate ($TBAPF_6$) was purified by recrystallization from ethyl acetate and dried *in vacuo* at 60 °C. All other chemicals were used as received unless otherwise stated. ^1H and ^{13}C NMR spectra were recorded on Varian Unity 300 MHz and Bruker-DRX 300 MHz spectrometers. Mass spectra were obtained on a JEOL JMS-SX 102A mass spectrometer. Differential scanning calorimetry (DSC) was performed on a SEIKO EXSTAR 6000DSC unit at a heating rate of 10 °C min^{-1} and a cooling rate of 40 °C min^{-1}. Samples were scanned from 30 to 400 °C, cooled to 0 °C, and then scanned again from 30 to 400 °C. The glass transition temperatures (T_g) were determined from the second heating scan. Thermogravimetric analysis (TGA) was undertaken on a DuPont TGA 2950 instrument. The thermal stability of the samples was determined under a nitrogen atmosphere, by measuring weight loss while heating at a rate of 20 °C min^{-1}. UV–Visible spectra were measured using an HP 8453 diode-array spectrophotometer. Photoluminescence (PL) spectra were obtained on a Hitachi F-4500 luminescence spectrometer. Cyclic voltammetry (CV) measurements were performed using a BAS 100 B/W electrochemical analyzer. The oxidation and reduction measurements were undertaken,

† Electronic supplementary information (ESI) available: DSC curves for spiro-**PAQ-Me** and spiro-**PAQ-Ph**. See http://www.rsc.org/suppdata/jm/b4/b402584a/

DOI: 10.1039/b402584a

respectively, in anhydrous CH_2Cl_2 and anhydrous THF containing 0.1 M $TBAPF_6$ as the supporting electrolyte, at a scan rate of 50 mV s^{-1}. The potentials were measured against an Ag/Ag^+ (0.01 M $AgNO_3$) reference electrode with ferrocene as the internal standard. The onset potentials were determined from the intersection of two tangents drawn at the rising current and background current of the cyclic voltammogram.

Fabrication of light-emitting devices

The hole-transport materials 4,4′-bis[*N*-(1-naphthyl)-*N*-phenylamino]biphenyl (NPB)[32] and 4,4′-dicarbazolyl-1,1′-biphenyl (CBP)[32] and the electron-transport material 1,3,5-tris(*N*-phenylbenzimidazol-2-yl)benzene (TPBI)[39] were synthesized according to literature procedures and sublimed through a temperature-gradient sublimation system. Pre-patterned ITO glasses that have active device areas of 3.14 mm^2 were cleaned thoroughly by sonication in detergent, ethanol, and DI water, successively, each time for 5 min. After being blown dry under a stream of nitrogen, the glasses were treated with oxygen plasma for 3 min and then loaded into an Ulvac Cryogenic deposition system, which was subsequently evacuated to a pressure below *ca.* 2×10^{-5} Torr. All of the organic layers were deposited at a rate of 1.5–2.5 Å sec^{-1}. For doped layers, the dopant and the host were co-evaporated from two separated boats with the rates controlled independently. An alloy of magnesium and silver (*ca.* 10 : 1, 50 nm) was deposited as the cathode, followed by a silver cap (1000 Å). The current–voltage luminance of each device was measured using a Keithley 2400 Source meter and a Newport 1835C Optical meter equipped with an 818ST silicon photodiode.

Synthesis of spiro-PAQ-Me

A mixture of compound **3** (2.00 g, 3.61 mmol) and 1,3-dimethyl-5-pyrazolone (**4**; 1.62 g, 14.4 mmol) in ethylene glycol (15.0 mL) was heated at 190 °C for 12 h. After cooling, the resulting mixture was poured into water (100 mL). The precipitated solid was collected by filtration, washed with water, and purified by column chromatography (hexane–ethyl acetate, 3 : 1) to afford **spiro-PAQ-Me** (1.88 g, 73.7%). ^1H NMR ($CDCl_3$): δ 8.09 (s, 2 H), 7.81 (d, J = 7.6 Hz, 2 H), 7.69–7.62 (m, 6 H), 7.56–7.47 (m, 6 H), 7.33 (dd, J = 7.2, 7.2 Hz, 2 H), 7.11 (dd, J = 7.2, 7.2 Hz, 2 H), 6.83 (d, J = 7.6 Hz, 2 H), 4.00 (s, 6 H), 2.04 (s, 6 H). ^{13}C NMR ($CDCl_3$): δ 153.7, 149.3, 141.6, 140.7, 137.7, 135.4, 129.8, 129.7, 128.8, 128.4, 128.3, 128.2, 124.8, 123.2, 122.9, 120.7, 116.9, 114.9, 64.9, 33.3, 14.6. HRMS (*m*/*z*): [M^+] calcd. for $C_{49}H_{34}N_6$, 706.2845; found 706.2844. Anal. calcd. for $C_{49}H_{34}N_6$: C, 83.26; H, 4.85; N, 11.89. Found: C, 83.35; H, 5.00; N, 12.09%.

Synthesis of spiro-PAQ-Ph

A mixture of compound **3** (2.00 g, 3.61 mmol) and 1-phenyl-3-methyl-5-pyrazolone (**5**; 2.51 g, 14.4 mmol) in ethylene glycol (15.0 mL) was heated at 190 °C for 24 h. After cooling, the resulting mixture was poured into water (100 mL). The precipitated solid was collected by filtration, washed with water, and purified by column chromatography (hexane/ethyl acetate, 5 : 1). Recrystallization from $CHCl_3$ yielded **spiro-PAQ-Ph** (1.28 g, 42.7%). ^1H NMR ($CDCl_3$): δ 8.26 (d, J = 8.0 Hz, 4 H), 8.11 (s, 2 H), 7.84 (d, J = 7.8 Hz, 2 H), 7.70–7.66 (m, 6 H), 7.60–7.55 (m, 6 H), 7.38 (dd, J = 7.6, 7.5 Hz, 4 H), 7.36 (dd, J = 7.5, 6.8 Hz, 2 H), 7.13 (dd, J = 7.4, 7.6 Hz, 4 H), 6.82 (d, J = 7.6 Hz, 2 H), 2.11 (s, 6 H). ^{13}C NMR ($CDCl_3$): δ 153.5, 149.9, 149.7, 149.0, 144.5, 143.9, 140.6, 139.7, 138.5, 135.3, 130.0, 129.8, 129.0, 128.6, 128.5, 128.3, 125.0, 124.8, 124.0, 123.9, 120.9, 120.4, 116.9, 116.4, 65.1, 14.2. HRMS (*m*/*z*): [M^+] calcd. for $C_{59}H_{38}N_6$, 831.3236; found 831.3243. Anal. calcd. for $C_{59}H_{38}N_6$: C, 85.28; H, 4.61; N, 10.11. Found: C, 85.45; H, 4.77; N, 10.28%.

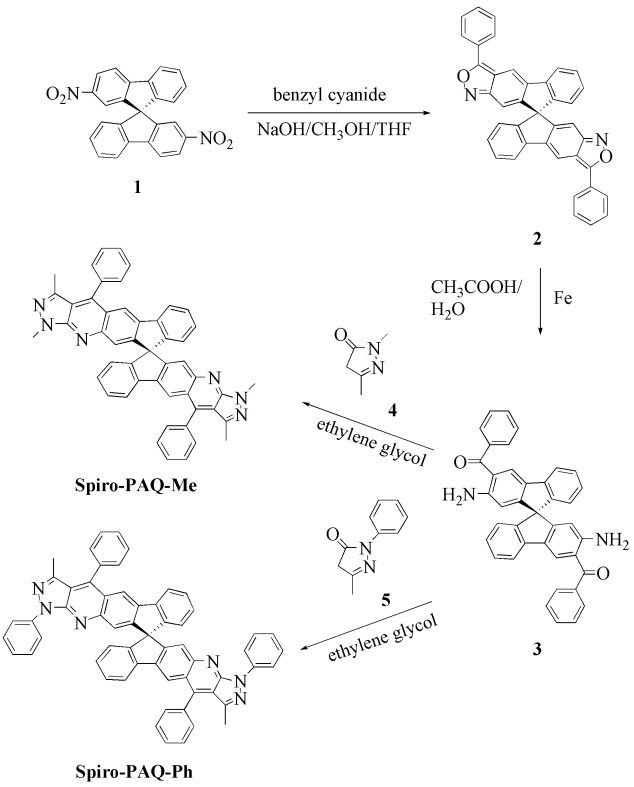

Scheme 1

Results and discussion

Synthesis

Scheme 1 illustrates the synthetic route followed for the preparation of the 9,9′-spirobifluorene-functionalized bis(pyrazoloquinoline)s. The key intermediate, 2,2′-diamino-3,3′-dibenzoyl-9,9′-spirobifluorene (**3**), was prepared from 2,2′-dinitro-9,9′-spirobifluorene (**1**) as reported previously.[36] The reaction of compound **1** with benzyl nitrile in the presence of base afforded the bisbenzisoxazole **2**, which was subsequently transformed into the bis(*o*-aminoketone) **3** by hydrogenation of the isoxazole moiety with an iron powder/acetic acid mixture. The condensation of **3** with pyrazolone derivatives **4** and **5**, respectively, in ethylene glycol yielded the target bis(pyrazoloquinoline)s spiro-**PAQ-Me** and spiro-**PAQ-Ph**, each containing a 9,9′-spirobifluorene skeleton. The chemical structures of the obtained spiro-bis(pyrazoloquinoline)s were confirmed by ^1H and ^{13}C NMR spectroscopy, mass spectrometry, and elemental analysis.

Optical properties

Fig. 1a displays the absorption and emission spectra of the spiro-**PAQ** dyes in EtOAc; their spectral data are summarized in Table 1. The absorption spectrum of spiro-**PAQ-Me** comprises a broad, low-energy absorption at ca. 420 nm, two weak absorptions in the region 340–360 nm, and a strong main absorption centered at 288 nm. In going from the methyl(spiro-**PAQ-Me**) to the phenyl-substituted (spiro-**PAQ-Ph**) bis(pyrazoloquinoline), there is a slight red-shift (2–6 nm) in position of the peak maximum, which is due to the increase in conjugation length. The features of these absorption spectra resemble those of the mono-pyrazoloquinoline (*i.e.* non-spiro) derivatives that have been described previously.[12] These spiro-**PAQ** dyes exhibit strong blue emissions: spiro-**PAQ-Me** displays an emission peak at 438 nm and a substitution effect, similar to that described above, is observed for the emission maximum; *i.e.* spiro-**PAQ-Ph** has an emission peak at 455 nm. We determined the solution fluorescence quantum

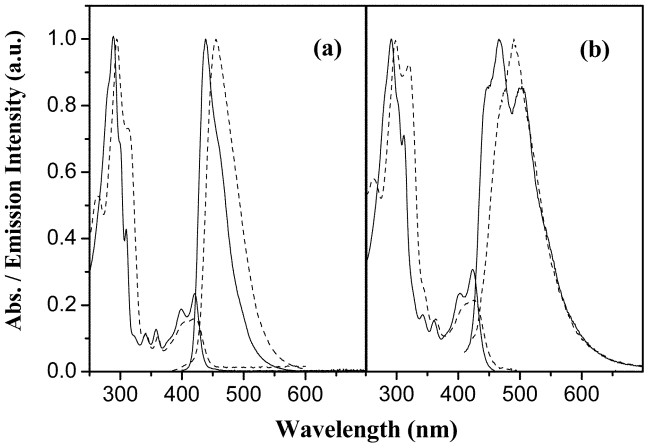

Fig. 1 UV–Vis absorption and PL spectra of spiro-**PAQ-Me** (—) and spiro-**PAQ-Ph** (– – –) (a) in EtOAc solution and (b) in the solid state.

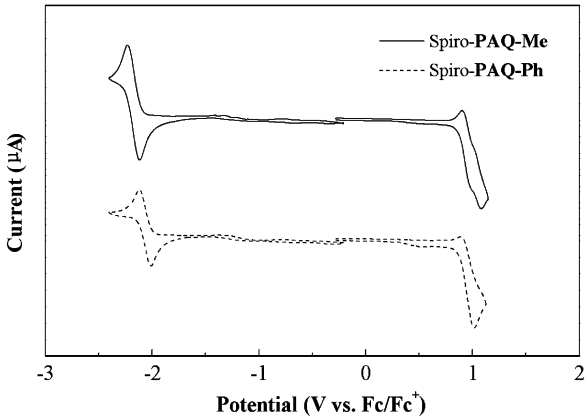

Fig. 2 Cyclic voltammograms of spiro-**PAQ-Me** and spiro-**PAQ-Ph**.

yields (Φ_f), 0.67 for the former and 0.95 for the latter, relative to that of 9,10-diphenylanthracene in cyclohexane (Φ_f = 0.90).[40] In comparison with their corresponding spectra in dilute solutions, the emission spectra of films of these spiro-**PAQ** derivatives, which were prepared by spin-coating on a glass substrate, are broadened and red-shifted by 30–35 nm. This phenomenon probably is due to the formation of intermolecular species, namely aggregates and excimers, in the solid state.

Thermal properties

We investigated the thermal properties of the spiro-bis(pyrazoloquinoline)s by differential scanning calorimetry (DSC) and thermogravimetric analysis (TGA). DSC was performed in the temperature range from 40 to 400 °C. Distinct glass transition temperatures (T_g) were observed at 246 and 280 °C for spiro-**PAQ-Me** and spiro-**PAQ-Ph**, respectively. Yet no crystallization or melting of the sample was observed up to 400 °C. In contrast, most of the monomeric PAQ dyes reported previously either do not exhibit a glass transition or have a low value of T_g (30–60 °C).[19,20] The prominent stability of the amorphous glass states of these spiro molecules may be due to the presence of their rigid, spiro-fused, orthogonal bifluorene linkages. In addition, the higher molecular weights of the bis(pyrazoloquinoline)s, relative to those of their monomers, may also play a role in raising their glass transition temperatures. Also evidenced by thermogravimetric analysis, both spiro-**PAQ-Me** and spiro-**PAQ-Ph** exhibit high thermochemical stability, with their 5%-weight-loss temperatures under a nitrogen atmosphere at 410 °C for the former and 512 °C for the latter. Apparently the introduction of spirobifluorene unit effectively improves both morphological and chemical stability of the pristine pyrazoloquinoline compounds.

Electrochemistry

We investigated the electrochemical behavior of the spiro-**PAQ** dyes by cyclic voltammetry using ferrocene as the internal standard. The results are displayed in Fig. 2 and the data are tabulated in Table 2. Cyclic voltammetry provides a simple method for obtaining the HOMO/LUMO energy levels of these materials, which we calculated with regard to the energy level of the ferrocene reference (4.8 eV below the vacuum level).[41] Upon cathodic scans, spiro-**PAQ-Me** and spiro-**PAQ-Ph** exhibit reversible reductions with onset potentials at *ca.* −2.09 and −2.00 V, respectively. During the anodic sweep, they undergo quasi-reversible oxidation processes with onset potentials at 0.87 V for the former and 0.86 V for the latter. Based on the onset potentials for the oxidation and reduction processes, we estimate the HOMO and LUMO energy levels of the spiro-**PAQ** dyes, which are summarized in Table 2. Also included in the Table is the band gap calculated from the absorption edge. A small deviation (0.13 eV or less) from the band gap calculated from electrochemical data is observed. The low-lying LUMO energy levels, which originate from the electron-deficient nature of the pyrazoloquinoline ring, are similar to those reported for dipyrazolopyridine derivatives.[21]

Electroluminescent devices

To investigate the electroluminescence properties of the spiro-bis(pyrazoloquinoline)s, we selected spiro-**PAQ-Ph**, which has the higher PL quantum yield and better thermal properties, for the OLED fabrication. We fabricated multilayer devices with

Table 1 Spectral data of spiro-pyrazoloquinolines

	λ_{max}[a]/nm	λ_{em},[b]/nm	λ_{max}/nm (film)[c]	Quantum yields (Φ)[a,d]
Spiro-**PAQ-Me**	288, 340, 358, 398, 420	438	466, 501 (sh)	0.67
Spiro-**PAQ-Ph**	294, 342, 361, 402, 422	455	490	0.95

[a] In EtOAc. [b] In EtOAc, excited at 360 nm. [c] Spin-coating from their $CHCl_3$ solution, excited at 360 nm. [d] The relative quantum yield was measured with reference to 9,10-diphenylanthracene in cyclohexane (Φ = 0.90).

Table 2 Electrochemical properties of spiro-pyrazoloquinolines

	E_{onset}^{ox}/V[a]	E_{onset}^{red}/V[a]	HOMO/eV[b]	LUMO/eV[c]	E_g^{el}/eV[d]	E_g^{opt}/eV[e]
Spiro-**PAQ-Me**	0.87	−2.09	5.67	2.71	2.96	2.83
Spiro-**PAQ-Ph**	0.86	−2.00	5.66	2.80	2.86	2.81

[a] Potential values referenced *vs.* Fc/Fc^+. [b] Determined from the onset oxidation potential. [c] Determined from the onset reduction potential. [d] Electrochemical band gap, estimated using the equation $E_g^{el} = E_{onset}^{ox} - E_{onset}^{red}$. [e] Optical band gap, calculated from the absorption edge of the absorption spectrum.

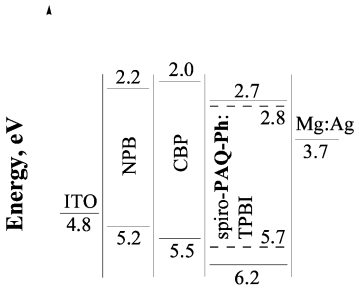

Fig. 3 Relative HOMO/LUMO energy levels of NPB, CPB, TPBI, spiro-**PAQ-Ph**, and other materials used in this study.

the configuration ITO/NPB (40 nm)/CBP (10 nm)/TPBI: *x*% spiro-**PAQ-Ph** (20 nm)/TPBI (20 nm)/Mg : Ag, where ITO, NPB, CBP, TPBI, and Mg:Ag denote indium tin oxide; 4,4′-bis[*N*-(1-naphthyl)-*N*-phenylamino]biphenyl; 4,4′-dicarbazolyl-1,1′-biphenyl; 2,2′,2″-(benzene-1,3,5-triyl)tris[1-phenyl-1H-benzimidazole]; and magnesium : silver alloy (*ca.* 10 : 1), respectively. Fig. 3 displays the relative HOMO/LUMO energy levels of NPB, CPB, TPBI, spiro-**PAQ-Ph**, and the other materials used in this study. Two layers of hole-transporting materials, NPB and CBP, were used because it has been demonstrated previously that CBP serves to provide an intermediate HOMO level by which holes can pass to the TPBI layer.[42,43] TPBI was chosen as a host material for the **PAQ-Ph** derivative because it is a wide band-gap material that emits strongly at *ca.* 376 nm.[42] From the analysis of the emission/absorption spectra of TPBI and spiro-**PAQ-Ph** (Fig. 1), we obtained reasonable spectral overlap and, thus, there exists an efficient Forster energy transfer from TPBI and the **PAQ-Ph** dye.

When the concentration of spiro-**PAQ-Ph** in TPBI was varied from 1.0 to 5.0 wt%; EL emission with a λ_{max} around 460 nm was observed, together with a shoulder of different intensity depending on the concentration, as shown in Fig. 4. In the absence of dopant, the device presents a broad EL spectrum that has a major contribution from TPBI (*ca.* 380 nm), a minor contribution from NPB (*ca.* 450 nm), and possibly an emission from CBP, which occurs at *ca.* 390 nm.[32] This observation indicates that the recombination region is located mainly in the TPBI region with some excitons formed in the NPB area. At dopant concentrations of 1.0–2.0 wt%, the devices exhibit bright blue emissions, predominantly arising from the dopant, as revealed from a comparison of the EL spectra with the PL spectrum of spiro-**PAQ-Ph**, together with a very minor contribution from the emission of TPBI host that is due to the incomplete energy transfer. Increasing the doping level to 5.0 wt% results in complete energy transfer. The performances of the devices are summarized in Table 3, and the current–voltage–luminance (*I*–*V*–*L*) characteristics of the device having a 2.0-wt% dopant concentration is presented in Fig. 5. For this 2.0%-doped device, the emission begins at *ca.* 3.5 V and reaches a maximum luminescence of 19 800 cd m^{-2} at *ca.* 15 V. With a current density of 20 mA cm^{-2} at 7.0 V, the device displayed

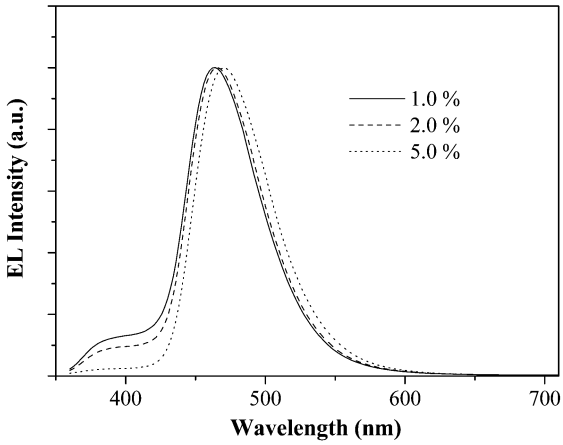

Fig. 4 Normalized electroluminescence spectra of ITO/NPB/CBP/TPBI:spiro-**PAQ-Ph** (x-wt%)/TPBI/Mg:Ag devices. The applied voltage was *ca.* 8.0 V.

high external quantum and luminescence efficiencies of 3.6% and 4.5 cd A^{-1} (2.02 lm W^{-1}), respectively, with CIE coordinates of $x = 0.14$ and $y = 0.17$. We note that the external quantum efficiency drops when increasing the dopant concentration from 2.0 to 5.0 wt%. This finding may be due to self-quenching of the dopant emission at higher concentration, but the external quantum efficiency still remains at *ca.* 3.0%.

Conclusions

In summary, we have synthesized spirobifluorene-based pyrazoloquinolines, spiro-**PAQ-Me** and spiro-**PAQ-Ph**, by the condensation of 2,2′-diamino-3,3′-dibenzoyl-9,9′-spirobifluorene (**3**) with pyrazolone derivatives, and have discussed details of their thermal properties, electronic properties (*viz.* absorption and photoluminescence), and electrochemical behavior. The presence of the rigid spirobifluorene skeleton imparts

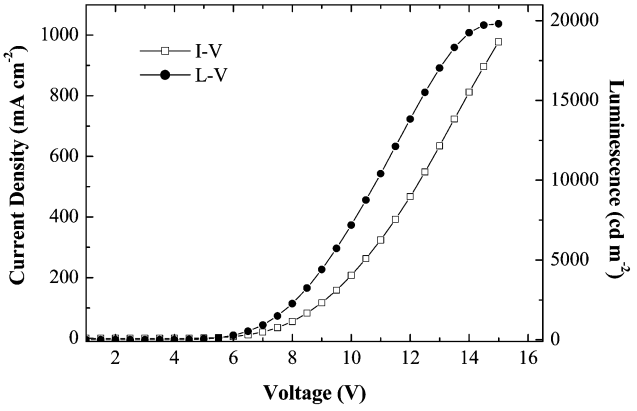

Fig. 5 Current–voltage characteristics and luminescence–voltage characteristics of an ITO/NPB/CBP/TPBI: spiro-**PAQ-Ph** (2.0-wt%)/TPBI/Mg:Ag device.

Table 3 Performance of ITO/NPB/CBP/TPBI:spiro-PAQ-Ph (x-wt%)/TPBI/Mg:Ag devices

Doping concentration (wt%)	1.0	2.0	5.0
Turn-on voltage/V[a]	3.4	3.5	3.5
Voltage/V[b,c]	6.7 (8.6)	7.0 (8.8)	6.8 (8.5)
Brightness/cd m^{-2}[b,c]	850 (3637)	892 (3816)	905 (3899)
Current efficiency/cd A^{-1}[b,c]	4.25 (3.64)	4.46 (3.82)	4.53 (3.90)
External quantum efficiency (%)[b,c]	3.67 (3.13)	3.55 (3.05)	2.99 (2.56)
Maximum brightness/cd m^{-2}	16 940 @14.5V	19 800 @15V	23 670 @15V
EL maximum/nm[d]	464	466	470
CIE coordinates, *x* and *y*[d]	0.14 and 0.15	0.14 and 0.17	0.14 and 0.21

[a] Recorded at 1.0 cd m^{-2}. [b] Recorded at 20 mA cm^{-2}. [c] The data in parentheses were recorded at 100 mA cm^{-2}. [d] Recorded at 8.0 V.

significant increases in these materials' glass transition temperatures, while preserving the optical and electrochemical characteristics of their pristine pyrazoloquinoline units. Multilayer EL devices having ITO/NPB/CBP/TPBI:spiro-**PAQ-Ph**/TPBI/Mg:Ag configurations display bright blue emissions, with luminescence intensities exceeding 20 000 cd m^{-2}, caused by the spirobifluorene-based pyrazoloquinoline dopant. At a 2.0 wt% doping level, the device possesses good blue purity, with an EL emission maximum at 466 nm, which corresponds to (0.14, 017) blue chromaticity in CIE coordinates, and exhibits a high luminescence efficiency of 4.5 cd A^{-1} (2.02 lm W^{-1}) at a current density of 20 mA cm^{-2} and a voltage of 7.0 V.

Acknowledgements

We thank the National Science Council of the Republic of China for financial support.

References

1 C. W. Tang and S. A. Van Slyke, *Appl. Phys. Lett.*, 1987, **51**, 913.
2 *Organic Electroluminescent Materials and Devices*, ed. S. Miyata and H. S. Nalwa, Cordon and Breach Publishers, New York, 1997.
3 C. H. Chen, J. Shi and C. W. Tang, *Macromol. Symp.*, 1997, **125**, 1.
4 C. H. Chen, J. Shi and C. W. Tang, *Coord. Chem. Rev.*, 1998, **171**, 161.
5 U. Mitschke and P. Bauerle, *J. Mater. Chem.*, 2000, **10**, 1471.
6 L. S. Hung and C. H. Chen, *Mater. Sci. Eng., R.*, 2002, **39**, 143.
7 J. Kido, K. Hongawa, K. Okuyama and K. Nagai, *Appl. Phys. Lett.*, 1994, **64**, 815.
8 J. Kido, H. Shionoya and K. Nagai, *Appl. Phys. Lett.*, 1995, **67**, 2281.
9 F. C. Chen, Y. Yang, M. E. Thompson and J. Kido, *Appl. Phys. Lett.*, 2002, **80**, 2308.
10 G. Gu and S. R. Forrest, *IEEE J. Sel. Top. Quantum Electron.*, 1998, **4**, 83.
11 Z. Yan and S. K. Wu, *J. Photochem. Photobiol.*, 1992, **66**, 69.
12 Z. He, G. H. W. Milburn, K. J. Baldwin, D. A. Smith, A. Danel and P. Tomasik, *J. Lumin.*, 2000, **86**, 1.
13 J. Niziol, A. Danel, G. Boiteux, J. Davenas, B. Jarosz, A. Wisla and G. Seytre, *Synth. Met.*, 2002, **127**, 175.
14 X. C. Gao, H. Cao, L. Q. Zhang, B. W. Zhang, Y. Cao and C. H. Huang, *J. Mater. Chem.*, 1999, **9**, 1077.
15 Z. He, G. H. W. Milburn, A. Danel, A. Puchala, P. Tomasik and D. Rasala, *J. Mater. Chem.*, 1999, **9**, 2323.
16 Z. Q. Gao, C. S. Lee, I. Bello, S. T. Lee, S. K. Wu, Z. L. Yan and X. H. Zhang, *Synth. Met.*, 1999, **105**, 141.
17 E. Balasubramaniam, Y. T. Tao, A. Danel and P. Tomasik, *Chem. Mater.*, 2000, **12**, 2788.
18 X. H. Zhang, W. Y. Lai, Z. Q. Gao, T. C. Wong, C. S. Lee, H. L. Kwong, S. T. Lee and S. K. Wu, *Chem. Phys. Lett.*, 2000, **320**, 77.
19 Y. T. Tao, E. Balasubramaniam, A. Danel, A. Wilsla and P. Tomasik, *J. Mater. Chem.*, 2001, **11**, 768.
20 Y. T. Tao, E. Balasubramaniam, A. Danel, B. Jarosz and P. Tomasik, *Chem. Mater.*, 2001, **13**, 1207.
21 Y. T. Tao, C. H. Chuen, C. W. Ko and J. W. Peng, *Chem. Mater.*, 2002, **14**, 4256.
22 R. Wu, J. S. Schumm, D. L. Pearson and J. M. Tour, *J. Org. Chem.*, 1996, **61**, 6906.
23 S. C. Wu and C. F. Shu, *J. Polym. Sci., Part A: Polym. Chem.*, 2003, **41**, 1160.
24 J. Salbeck, N. Yu, J. Bauer, F. Weissörtel and H. Bestgen, *Synth. Met.*, 1997, **91**, 209.
25 J. Salbeck, J. Bauer and F. Weissörtel, *Macromol. Symp.*, 1997, **125**, 121.
26 N. Johansson, D. A. dos Santos, S. Guo, J. Cornil, M. Fahlman, J. Salbeck, H. Schenk, H. Arwin, J. L. Brédas and W. R. Salenek, *J. Chem. Phys.*, 1997, **107**, 2542.
27 N. Johansson, J. Salbeck, J. Bauer, F. Weissörtel, P. Bröms, A. Andersson and W. R. Salaneck, *Adv. Mater.*, 1998, **10**, 1136.
28 H. Tian, B. Chen and P. –H. Liu, *Chem. Lett.*, 2001, 990.
29 W. J. Shen, R. Dodda, C. C. Wu, F. I. Wu, T. H. Liu, H. H. Chen, C. H. Chen and C. F. Shu, *Chem. Mater.*, 2004, **16**, 930.
30 M. D. Joswick, I. H. Cambell, N. N. Barashkov and J. P. Ferraris, *J. Appl. Phys.*, 1996, **80**, 2883.
31 S. Tokito, H. Tanaka, K. Noda, A. Okada and Y. Taga, *Appl. Phys. Lett.*, 1997, **70**, 1929.
32 B. E. Konne, D. E. Loy and M. E. Thompson, *Chem. Mater.*, 1998, **10**, 2235.
33 D. F. O'Brien, P. E. Burrows, S. R. Forrest, B. E. Konne, D. E. Loy and M. E. Thompson, *Adv. Mater.*, 1998, **10**, 1108.
34 F. Steuber, J. Staudigel, M. Stössel, J. Simmerer, A. Winnacker, H. Spreitzer, F. Weissörtel and J. Salbeck, *Adv. Mater.*, 2000, **12**, 130.
35 Y. Shirota, *J. Mater. Chem.*, 2000, **10**, 1.
36 C. L. Chiang and C. F. Shu, *Chem. Mater.*, 2002, **14**, 682.
37 F. I. Wu, R. Dodda, D. S. Reddy and C. F. Shu, *J. Mater. Chem.*, 2002, **12**, 2893.
38 J. H. Weisburger, E. K. Weisburger and F. E. Ray, *J. Am. Chem. Soc.*, 1950, **72**, 4253.
39 J. Shi, C. W. Tang and C. H. Chen, U.S. Patent 5,645,948,/1997.
40 D. Eaton, *Pure Appl. Chem.*, 1998, **60**, 1107.
41 J. Pommerehne, H. Vestweber, W. Guss, R. F. Mahrt, H. Bässler, M. Porsch and J. Daub, *Adv. Mater.*, 1995, **7**, 551.
42 Y. T. Tao, E. Balasubramaniam, A. Danel and P. Tomasik, *Appl. Phys. Lett.*, 2000, **77**, 933.
43 Z. Zhang, X. Jiang and S. Xu, *Thin Solid Films*, 2000, **363**, 61.